INTERNATIONAL JOURNAL OF INTEGRATED ENGINEERING
ISSN: 2229-838X e-ISSN: 2600-7916

IJIE

Vol. 17 No. 2 (2025) 222-234
https://publisher.uthm.edu.my/ojs/index.php/ijie

Non-Destructive Method for Moisture Content Sensing Inside a Rice Storage

Nurul Amira Mohd Ramli[1], Mohd Hafiz Fazalul Rahiman[2,3]*, Latifah Munirah Kamarudin[3,4], Latifah Mohamed[2,3], Ammar Zakaria[2,3], Mohammed Saeed Moqbel Abdullah[2], Ruzairi Abdul Rahim[5]

[1] *Faculty of Engineering and Science, Curtin University Malaysia, Miri, 98009, MALAYSIA*
[2] *Faculty of Electrical Engineering and Technology, Universiti Malaysia Perlis, Arau, 02600, MALAYSIA*
[3] *Centre of Excellence for Advanced Sensor Technology, Universiti Malaysia Perlis, Arau, 02600, MALAYSIA*
[4] *Faculty of Electronic Engineering and Technology, Universiti Malaysia Perlis, Arau, 02600, MALAYSIA*
[5] *Faculty of Electrical and Electronic Engineering, Universiti Tun Hussein Onn Malaysia, Parit Raja, Batu Pahat Johor, 86400, MALAYSIA*

*Corresponding Author: hafiz@unimap.edu.my
DOI: https://doi.org/10.30880/ijie.2025.17.02.018

Article Info

Received: 23 October 2024
Accepted: 14 July 2025
Available online: 28 July 2025

Keywords

Image reconstruction, moisture content, radio tomographic imaging, received signal strength, rice moisture content

Abstract

Rice grains represent the majority of worldwide consumed daily food, especially for most countries in Asia, where rice crops symbolize the feature of the local culture. However, as rice grains are naturally hygroscopic, the total values (quality and quantity) are degrading due to their varying level of moisture content. Currently, a sampling moisture sensing based on a single-point measurement is employed to monitor the moisture content level. In this scenario, the conventional method needs to be revised because it is very localized and only represents part of the moisture distribution inside the bulk grains. Besides, implementing several high-end technologies is considerably expensive for small-scale industries in developing countries. Therefore, this study has developed an RTI system in a prototype scale for a constructive moisture sensing method. RTI is a unique approach that reconstructs an image across the monitored WSN area by exploiting the attenuation of RF signals caused by the presence of targeted subjects. Five rice moisture profiles at the percentage of 15%, 20% and 25% were reconstructed using image reconstruction algorithms, LBP, FBP, NOSER and TR. This study analyses the effectiveness of the proposed method in both simulation and experimental studies. The results positively support the possibility of engaging the RTI technique to localize the moisture distribution in rice storage.

1. Introduction

Paddy grains are routinely harvested for a maximum yield when the moisture content ranges between 18 – 25% [1, 2]. Then the grains are cleaned and processed to remove impurities, such as rotten seeds, paddy straws and stones. Before loading the paddy and rice grains for safe storage, their moisture content must be reduced on average by 12 – 14%, depending on the local weather conditions, storage conditions, and types of storage [3–5].

According to a review by [6], moisture content plays a crucial role in modifying the physicochemical attributes of grains, potentially impacting their overall quality. Thus, the former drying process becomes mandatory because the extended storage period and different purposes in managing and marketing the grains would necessitate different ranges of percentages of moisture content.

Throughout the storage period, the quality of the rice grains cannot be improved. The reinforcement of air dryers to regulate moisture content has proven beneficial in enhancing silo aeration, consequently preserving grains with minimal quality loss throughout the storage duration. Nevertheless, previous studies have highlighted that the moisture content increases with increasing storage period, which later results in rice grains deterioration, development of fungal attacks, additional drying cost, and reduction in the commercial values [7, 8]. Besides, in Malaysia, for example, measuring the percentage and localising the distribution of rice moisture content throughout the storage process is challenging due to the monsoonal effect, which can be classified as a wet-humid climate with a relative humidity of approximately 80% [5].

Until now, the percentage of rice moisture content has been commonly measured using primary and secondary methods. The primary method applies the traditional sensing of absolute moisture in grains through the standard oven-drying process [9]. In contrast, the second method uses either a straightforward and convenient moisture meter or high-end technologies [10]. Although the primary method is constantly reliable, this technique involves complex procedures and is time-consuming, making it unsuitable for real-time measurement. In addition, this technique executes gravimetric analysis, which is a destructive process that eventually reduces the grains' quantity throughout the storage period. Meanwhile, the second method is more favourable because this technique is straightforward, non-destructive and provides rapid measurement. Even so, some measurement approaches are impractical for moisture sensing on a silo scale. The failure is due to the single-point measurement, meaning that the measured moisture content does not represent the distribution of moisture within the bulk grain inside the silo. Furthermore, the cost of implementing advanced technology in developing countries is considerably high [11, 12].

Therefore, this comprehensive study designs and develops a radio tomographic imaging (RTI) system to improve the efficiency and accuracy of moisture distribution sensing in rice storage. RTI is a unique approach that images the subject's location based on the attenuation in radio frequency (RF) signals from a measured baseline value obtained from the links between each stationary sensor node within a wireless network area. The proposed method focuses on tomogram analysis produced by employing the RTI technique for sensor data collection, reconstructing the image of interest through several image reconstruction algorithms and utilising several image quality assessments to evaluate the effectiveness of the proposed method. The findings could lead to more exploration of the feasibility of an RTI system as a tool for sensing the changes in grains' moisture content, which subsequently establishes a new approach for a reliable, non-destructive and online sensing method.

2. System Configuration

RTI technique is currently the most engaging approach for Device-Free Localization (DFL) technology [13]. The RF sensing principle has led to the establishment of the RTI approach, which eventually evolved as one of the most efficient localisation techniques. Across the monitoring wireless sensor network (WSN), this RTI system practically works by exploiting the attenuation of RF signals, in terms of received signal strength (RSS) quality, caused by the presence of targeted objects. RSS-based measurement has been extensively used in WSN monitoring and localisation systems because it does not involve the installation of new hardware for the system development, as it is already equipped with RF sensor nodes. The original concept of RSS measurements for the RTI imaging system was proposed by [14], where they computed these RSS losses to reconstruct the cross-sectional image inside the monitoring area.

Generally, a tomography system's structure can be visualised as three main components: the sensory system, data acquisition and image reconstruction and display system [15, 16]. Fig. 1 describes the structure of the RTI system for rice moisture sensing application, while Fig. 2 illustrates the hardware measurement setup. The RTI system includes a rice silo, an array of RF sensor nodes mounted externally on the silo's peripheral, a data acquisition system to measure the data from all sensor nodes and a personal computer for data processing and image reconstruction. A simulation modelling is carried out to analyse the spatial behaviour of a system, assess the image reconstruction results and summarise the fundamental findings. In this study, COMSOL Multiphysics software was utilised as a numerical approach using the FEM tool to model the RTI system. An experimental lab-scaled rice silo setup has been developed non-invasively to evaluate and validate the effectiveness of the RTI system for localisation and monitoring. The system used is non-invasive.

Int. Journal of Integrated Engineering Vol. 17 No. 2 (2025) p. 222-234

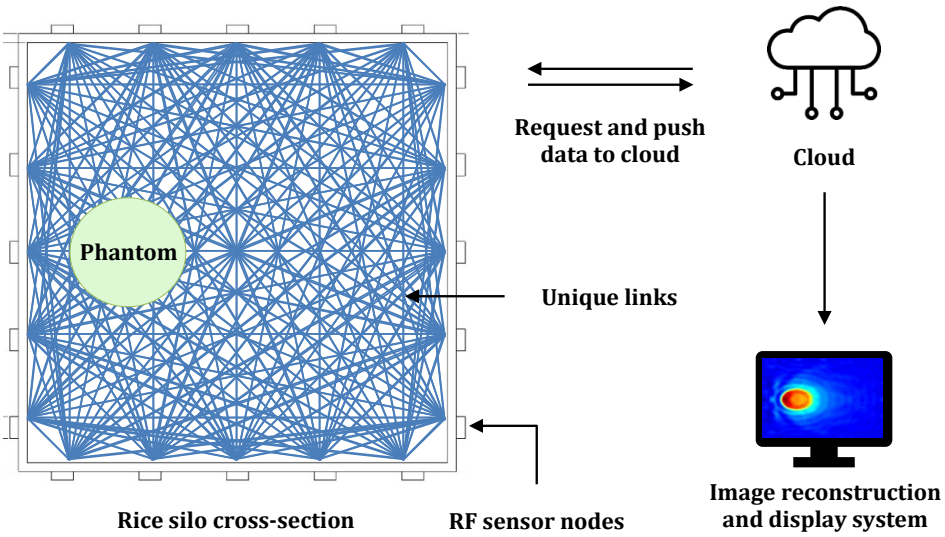

Fig. 1 *Structure of the RTI system*

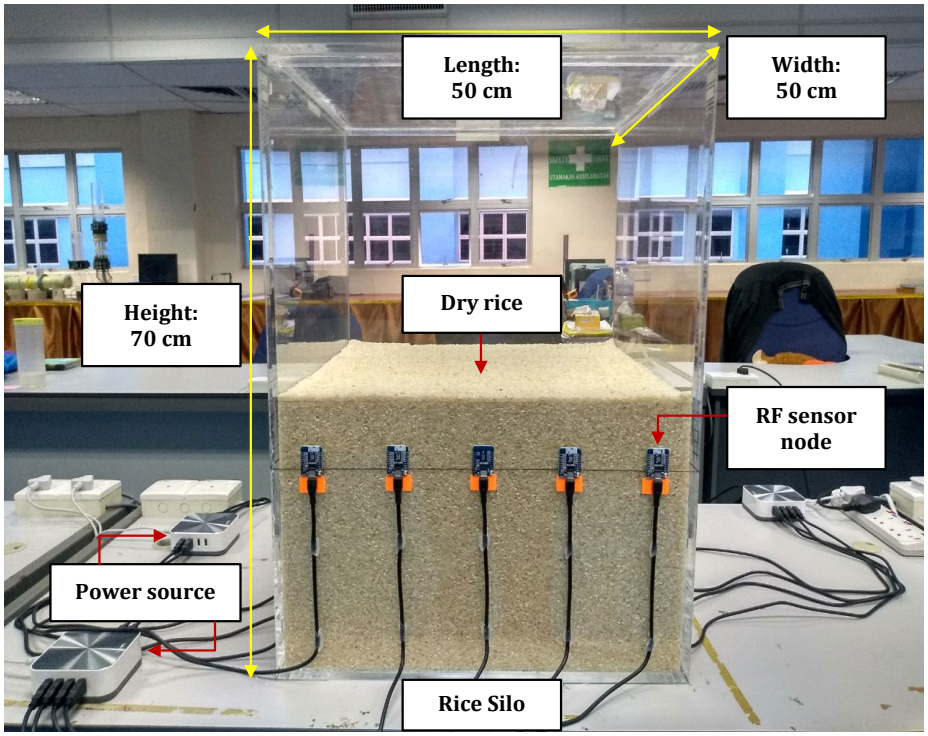

Fig. 2 *RTI measurement system set-up*

In this research, the rice silo is designed as a square shape made of an acrylic plate with a wall thickness of 1 cm. Polymethyl methacrylate (PMMA) is selected for its sturdiness in various applications [17]. The structure of the silo proposed in this initial study is designed to be 50 x 50 cm in square length and 70 cm in height. Since the radio propagation mechanism may include wave scattering, diffraction and reflection, the silo size is significantly considered relative to the wavelength of the propagating frequency to prevent electromagnetic wave interference inside the silo [18, 19]. Besides, as cited in reference [20], the attenuation of electromagnetic waves increases in correlation with the expansion of the monitoring area. Therefore, this dimension is specifically chosen to investigate the capability of the RTI technique to image the moisture distribution inside the rice silo.

The rice silo system is also configured with 20 RF sensor nodes located evenly along the boundary of the square rice silo, with an operating frequency of 2.4 GHz. The 2.4 GHz frequency is preferred to utilise the low-cost, over-the-shelf Wi-Fi sensor and standard ISM band of the WSN. On top of that, the 2.4 GHz frequency is very sensitive to moisture content, which eventually helps in reconstructing the image contrast. The RF sensor nodes are arranged in such a way as to receive the scattered electric fields in multiple directions. In addition, the node

density also plays a significant role in the successful imaging results. Previous research has reported that employing 16 sensor nodes instead of 8 sensor nodes enhanced the quality of the reconstructed images [21]. Within the same monitoring area, [21] also concluded that a closer arrangement of sensor nodes is anticipated to yield better imaging results due to the increased number of projection links intersecting at the same point in the targeted area.

2.1 RF Sensor Nodes: Modelling and Simulation

Electromagnetic waves constitute measurable electric (E) and magnetic (M) fields, which must coexist. Over decades, the remarkable features of electromagnetic waves when propagating in a dielectric medium have led to the establishment of advanced and practical solutions, especially in wireless sensing or imaging [22]. In this study, the description of electromagnetism is expressed by Statistical Maxwell's Electromagnetic Theories, as shown by [15, 23].

It is necessary to have a mathematical model for the RF sensor node so that the RTI system can accommodate the simulation of silos at any size with a flexible number of sensor nodes. In this study, the sensor node is modelled as a rectangular waveguide operating at 2.4 GHz and TE_{10} directing wave mode. The width of the rectangular waveguide, w is modelled and calibrated through Eq. (1) [24]. Contrarily, the length of the RF node can be randomly drawn at a suitable size in the 2D overall plane [25].

$$f_c = \frac{c_o}{2w\sqrt{\varepsilon_r}} \tag{1}$$

Where f_c is the cut-off frequency depending on the width of the waveguide, w, c_o is the speed of light, 3 x 10^8 ms^{-1} and ε_r is the relative permittivity of dry rice. RF signals can propagate in the dry rice medium if the cut-off frequency is lower than the operating frequency. According to [26], in a practical operating range of TE_{10} mode, the cut-off frequency must be higher than 1.22 GHz and less than 2.45 GHz. Herein, the width, w of the RF node is 5.73 cm at a cut-off frequency of 1.37 GHz.

2.2 RF Sensor Nodes: Experimental Design

Since the RSS metric is course information and sensitive, the faulty deployment of RF sensor nodes in terms of elevation from the ground and distance between a transmitter and receiver exposes it to multipath effects and interference signals from the neighbouring sensor nodes [27]. This phenomenon is specified when the RF signals reach the receiver by two or more paths, mainly due to the ground reflections. Hence, the RF sensor nodes arrangement has been realised in a well-mannered environment, as in Eq. (2) [28]. Plus, to disregard the ground attenuation between the sensor nodes with a transmission frequency of 2.4 GHz, previous research has suggested that the sensor node's height should be much larger than the frequency wavelength ($h \gg \lambda$), and 0.8 m to 1.25 m height just fit for the adjacent sensor nodes placed at a distance less than 5 m [29, 30].

$$r = 17.32 \times \sqrt{\frac{d}{4f}} \tag{2}$$

Where r is the radius of the Fresnel zone, d is the maximum distance between a transmitter and receiver nodes (km) and f indicates the transmitted frequency (GHz). Based on the calculation, all rice moisture profiles should not be positioned 12.49 cm lower than the level of RF sensor nodes.

2.3 Rice Moisture Profiles Setting: Modelling and Simulation

Permittivity, or dielectric properties, are the electrical characteristics of poorly conducting materials that vary significantly with exposed electromagnetic waves. When interacting with RF, these properties are studied as the parameters that can be polarised by electromagnetic energy. Thus, this RTI system is based on the relationship between the electric field and the medium's dielectric properties. The relative complex permittivity of the rice is expressed in Eq. (3) [15, 31].

$$\varepsilon_r = \varepsilon' - j\varepsilon'' \tag{3}$$

Where ε' is the dielectric constant that describes the capability of a material to store energy in the electric field, and ε'' is the dielectric loss factor that indicates the capability of a material to dissipate energy from the electric field, which is then converted into heat energy.

Int. Journal of Integrated Engineering Vol. 17 No. 2 (2025) p. 222-234

The modelling of the rice grains is separated into two parts: the dry rice as a reference medium and the moisture rice that indicates the rice phantoms with 'X' moisture content. The dry rice is assumed to be at 14% moisture based on the standard moisture content level for rice storage following the drying process [1, 2]. For the rice phantoms, the MC is set incrementally by 5% each time it is increased, starting at 15%, 20% and finally, 25%. The most moisture phantom of 25% moisture demonstrated the worst condition for rice grains since the maximum moisture content of paddy grains post-harvesting process is 24% to 26% [1, 2]. Eq. (4) and (5) represent the correlation between complex dielectric properties of rice grains with moisture content based on the regression method modelled by these researchers [6, 32].

$$\varepsilon' = a_0' + a_1' MC + a_2' MC^2 \tag{4}$$

$$\varepsilon'' = a_0'' + a_1'' MC + a_2'' MC^2 \tag{5}$$

Where the value of coefficients a_0', a_1', a_2' and a_0'', a_1'', a_2'' are for the polynomial expression of the dielectric constant, ε' and dielectric loss factor, ε'', respectively. These coefficients are expressed as a function of frequency, f, as tabulated in Table 1.

Table 1 *Quadratic coefficients of equations (4) and (5)*

Dielectric properties	Coefficient functions
Dielectric constant, ε'	$a_0' = -0.4605f^2 + 8.5289f - 5.1708$
	$a_1' = 0.0544f^2 - 0.9928f - 0.2982$
	$a_2' = -0.0016f^2 + 0.0281f + 0.0224$
Dielectric loss factor, ε''	$a_0'' = 0.1347f^2 + 0.6010 - 8.4663$
	$a_1'' = -0.0166 - 0.0693f + 0.8215$
	$a_2'' = 0.0005f^2 + 0.0023f - 0.0149$

2.4 Rice Moisture Profiles Setting: Experimental Design

The valuable expense of the rice grains prevented this study from intentionally causing uncontrolled spoilage. Hence, the rice moisture profiles are placed inside cylindrical-shaped containers throughout the experimental study. This research introduces two sizes of plastic containers to represent the rice moisture profiles, as presented in Fig. 3. Although the containers are slightly different in height, the level of the rice moisture is maintained at about 22 cm for both containers. According to [33], the thickness of both containers (1 mm) compared to the wavelength of 2.4 GHz radiating frequency (124.91 mm) is negligible.

The percentage of moisture content is increased to the desired levels based on the moistening method used by the previous research in reference [34] and [35]. The difference in the percentage of moisture content can be achieved by adding a predetermined amount of water, Q in kg, as calculated by Eq. (6).

$$Q = \frac{W_i(M_d - M_i)}{(100 - M_d)} \tag{6}$$

Where W_i is the initial mass of the rice grains (kg), M_i is the initial percentage of the rice moisture content (% wet basis) and M_d is the desired percentage of the moisture profiles (% wet basis).

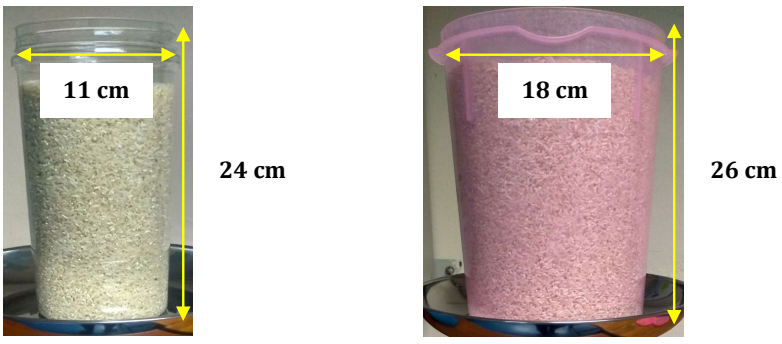

Fig. 3 *Details of the physical containers representing the rice moisture profiles*

3. Image Reconstruction Technique

3.1 Solving Forward Problem

This study exploited the transmission links within the RF sensor network to assess the RSS values. This RSS value, measured in dB, indicates the power of a received RF signal as it propagates through a medium from a transmitter to a receiver. From a line of sight (LOS) perspective, the transmission link deteriorates as it travels across a distance or crosses the attenuating object between the network area. Considering all the simultaneous transmission links in the RTI network area, the changes in RSS value, y can be formulated in a matrix form as in Eq. (7).

$$y = Wx + \Delta n \tag{7}$$

Where y is the vector of the measured RSS, W is the n x m weighting matrix, x is the expected attenuation image, which has to be determined and Δn is the noise vector.

The RSS measurement is recorded in two different conditions. Initially, the RTI system is calibrated when there is no rice moisture profile inside the silo. Then, the RSS data is collected when the moisture profile is inside the silo. Therefore, using the RTI-based technique, the difference between these two RSS measurements can be employed to localize the object of interest [36].

3.2 Solving Inverse Problem

The inverse problem is addressed to determine the unknown electric field distribution vector from the sensor data output [16]. Thus, in consequence of solving the forward problem that forms the weighting matrix, several image reconstruction algorithms have been used to reconstruct the attenuation mapping of the rice moisture profiles.

• Linear Back Projection (LBP)

LBP is a non-iterative algorithm well known for its simple computational procedure, enabling it to generate a tomogram at high speed [37]. Using the LBP algorithm, each normalized weighting matrix is multiplied by its corresponding sensor loss at a receiver i-th for projection j-th [38]. Then the individual multiplication is summed to attain the back-projected electric field distribution (concentration profile). The weighting matrix has been normalized to standardize the output matrices, as in Eq. (8). The following Eq. (9) lines the mathematical equation for the LBP algorithm.

$$\bar{J}_{ji} = \frac{J_{ji}}{W} \tag{8}$$

Where W is the total add-up of the weighting matrix, also known as the weight balance matrix.

$$G_{LBP}(x,y) = \sum_{j=1}^{20}\sum_{i=1}^{20} L_{ji} \times \bar{J}_{ji}(x,y) \tag{9}$$

Where L_{ji} is the sensor loss, $L_{ji} = S_{ji}^{tot} - S_{ji}^{inc}$. S_{ji}^{tot} is defined by the electric field that is measured when there is a rice moisture profile inside the monitoring area and S_{ji}^{inc} is the electric field measured before the presence of the moisture profile.

• Filtered Back Projection (FBP)

FBP is a mathematical approach to sharpen the previously reconstructed tomographic images using the LBP algorithm [37]. In the FBP algorithm, a filter matrix, F having the dimension as the weighting matrix, is introduced to contribute a weighting for each pixel. As a result, a uniform concentration profile is produced at equal sensor output. It is obtained by dividing the maximum pixel magnitude, P_{m} by the weight-balanced matrix, W as shown in Eq. (10).

$$F = \frac{P_m}{W} \tag{10}$$

Hence, the FBP algorithm is defined by multiplying the concentration profile derived using the LBP algorithm with a filter matrix, F as given in Eq. (11).

$$G_{FBP}(x,y) = F(x,y) \times G_{LBP}(x,y) \tag{11}$$

• Newton's One Step Error Reconstruction (NOSER)

NOSER is a fast and practical image reconstruction algorithm due to its stability and direct linear method [39]. The formulation of the NOSER algorithm is shown in Eq. (12).

$$G_{NOSER}(x,y) = [H]^T \times \sum_{j=1}^{20}\sum_{i=1}^{20} LS_{ji} \times \bar{J}_{ji}(x,y) \tag{12}$$

Where LS_{ji} is calculated as $LS_{ji} = \left[S_{ji}^{tot} - S_{ji}^{inc}\right]^2$ using the least square method. The least-square method aims to minimize the variation between the S_{ji}^{tot} and S_{ji}^{inc} for a given electric field distribution in the computational domain [24]. H is the Hessian matrix, $H = J_{ji}(x,y) * \left[J_{ji}(x,y)\right]^T$ which acts as the stabilizer and $J_{ji}(x,y)$ is the computed weighting matrix as describe above. In addition, the transposed Hessian matrix is utilized as a rough approximation instead of using an inverse matrix because it is impossible to compute the direct inverse [40].

• Tikhonov Regularisation (TR)

TR is a widely used algorithm [36] that provides a simple framework for integrating the desired features into tomographic images. In this study, the summation of the Hessian matrix was decomposed into three constituent matrices, which are U, V and Σ. U and V are the unitary matrices, and Σ is a diagonal matrix. The diagonal elements of Σ are singular values, ρ, as expressed in Eq. (13).

$$\rho = diag(\Sigma) \tag{13}$$

Based on Eq. (13), the involved regularization would introduce additional information into the mathematical model to handle these small singular values, hence stabilizing the inverse problem [41].

Tikhonov's smoothing approach is influenced by this regularization parameter, κ where $\kappa > 0$. The iteration is concluded to have reached its limitation when a constant value of the image quality assessment is recorded. Thus, the same κ value is chosen as the optimum regularization parameter to construct the rice moisture profiles.

$$T_{tikh,\kappa} = \frac{\rho}{\rho^2 + \kappa} \tag{14}$$

Eq. (15) below shows the mathematical representation of the TR algorithm used to reconstruct the image for this RTI system.

$$G_{tikh}(x,y) = U \times V \times diag(T_{tikh,\kappa}) \times \sum_{j=1}^{20}\sum_{i=1}^{20} LS_{ji} \times \bar{J}_{ji}(x,y) \tag{15}$$

4. Results and Discussions

This section objectively presents and discusses the results of the simulation and experimental studies according to the methodologies carried out in the earlier section. The capability of the tested RTI system is validated by imaging the rice moisture profiles utilizing the proposed image reconstruction algorithms. Fig. 4 illustrates the five positions of rice moisture profiles involving single and multiple positions. Profile A has a single small rice moisture with a diameter of 11 cm. Profile B depicts dual equal sizes of small rice moisture placed vertically with a diameter of 11 cm each. On the other hand, Profile C placed one big size of rice moisture with a diameter of 18 cm. Profile D displayed a position of the same size as two big rice moisture positioned horizontally, with a diameter of 18 cm. Lastly, Profile E portrays dual sizes of rice moisture placed vertically with a diameter of 11 cm and 18 cm each.

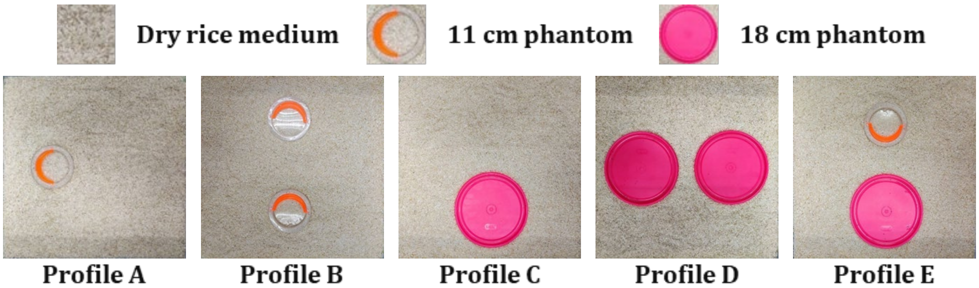

Fig. 4 *Positions of rice moisture profiles*

The image reconstruction outcomes from all rice moisture profiles studied utilising LBP, FBP, NOSER and TR algorithms are tabulated in Tables 2, 3, 4 and 5, respectively. Every simulated and experimental image is compared with its corresponding reference image. Despite the hampered smearing artefacts and noises, all four image reconstruction algorithms have adequately generated the imaging results as closely identical to the reference images with no discrepancies for the percentage of 15%, 20% and 25% of rice moisture content. It can be observed that the higher intensity spot (dark red colour) is more concentrated in the targeted location, which represents the rice moisture distribution.

As discovered in the tabulated results, these reconstructed images visualized that, as the number and size of the rice moisture increased, the smearing artefacts increasingly marked up the images, consequently promoting the image noise floor. The LBP and FBP algorithms mostly reflect this condition compared to the NOSER and TR algorithms. The LBP and FBP algorithms are well understood for their poor accuracy due to the appearance of artefacts conceivably caused by the back-projection techniques. In contrast, the NOSER and TR algorithms have visually improved the reconstructed tomogram images for all rice moisture profiles. The improvement in minimizing the smearing artefacts by these algorithms is likely yielded through solving the inverse problem using the non-linear approach.

Table 2 *Reconstructed images of rice moisture profiles using the LBP algorithm*

Reference image	15% Moisture content		20% Moisture content		25% Moisture content	
	Simulation	Experimental	Simulation	Experimental	Simulation	Experimental
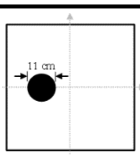	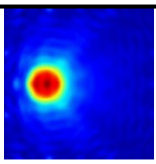	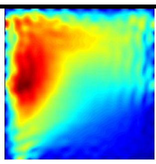	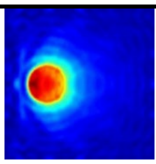	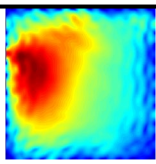	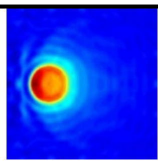	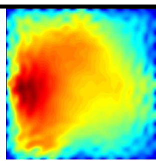
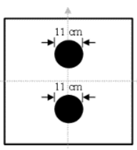	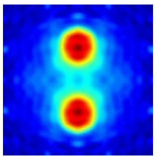	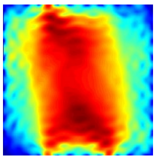	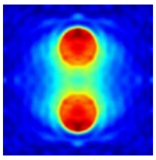	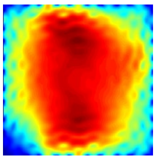	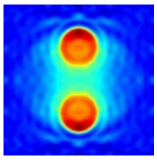	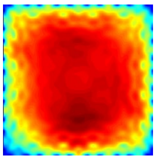
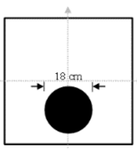	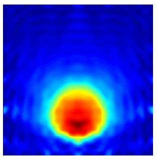	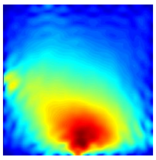	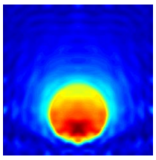	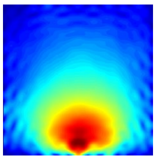	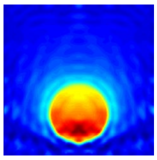	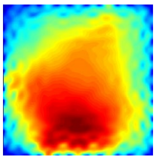
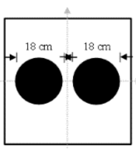	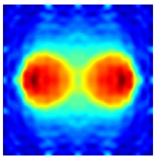	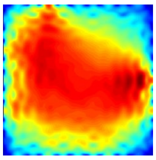	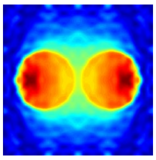	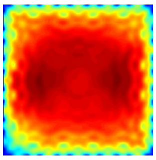	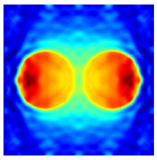	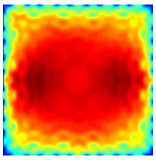
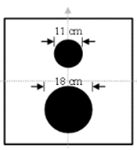	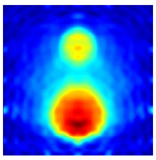	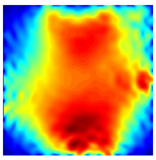	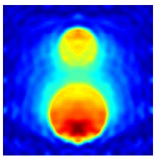	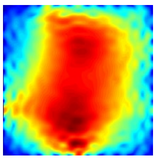	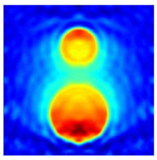	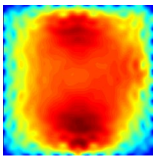

Int. Journal of Integrated Engineering Vol. 17 No. 2 (2025) p. 222-234

Table 3 *Reconstructed images of rice moisture profiles using the FBP algorithm*

Reference image	15% Moisture content		20% Moisture content		25% Moisture content	
	Simulation	Experimental	Simulation	Experimental	Simulation	Experimental
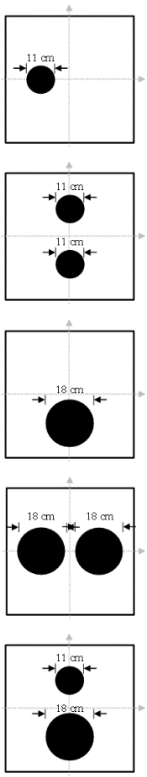						

Table 4 *Reconstructed images of rice moisture profiles using the NOSER algorithm*

Reference image	15% Moisture content		20% Moisture content		25% Moisture content	
	Simulation	Experimental	Simulation	Experimental	Simulation	Experimental
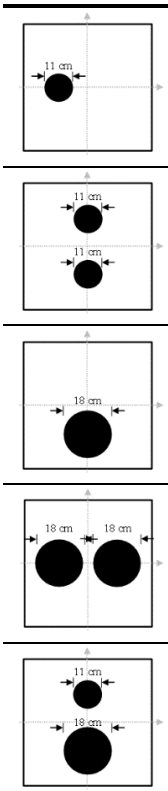						

Table 5 *Reconstructed images of rice moisture profiles using the TR algorithm*

Reference image	15% Moisture content		20% Moisture content		25% Moisture content	
	Simulation	Experimental	Simulation	Experimental	Simulation	Experimental

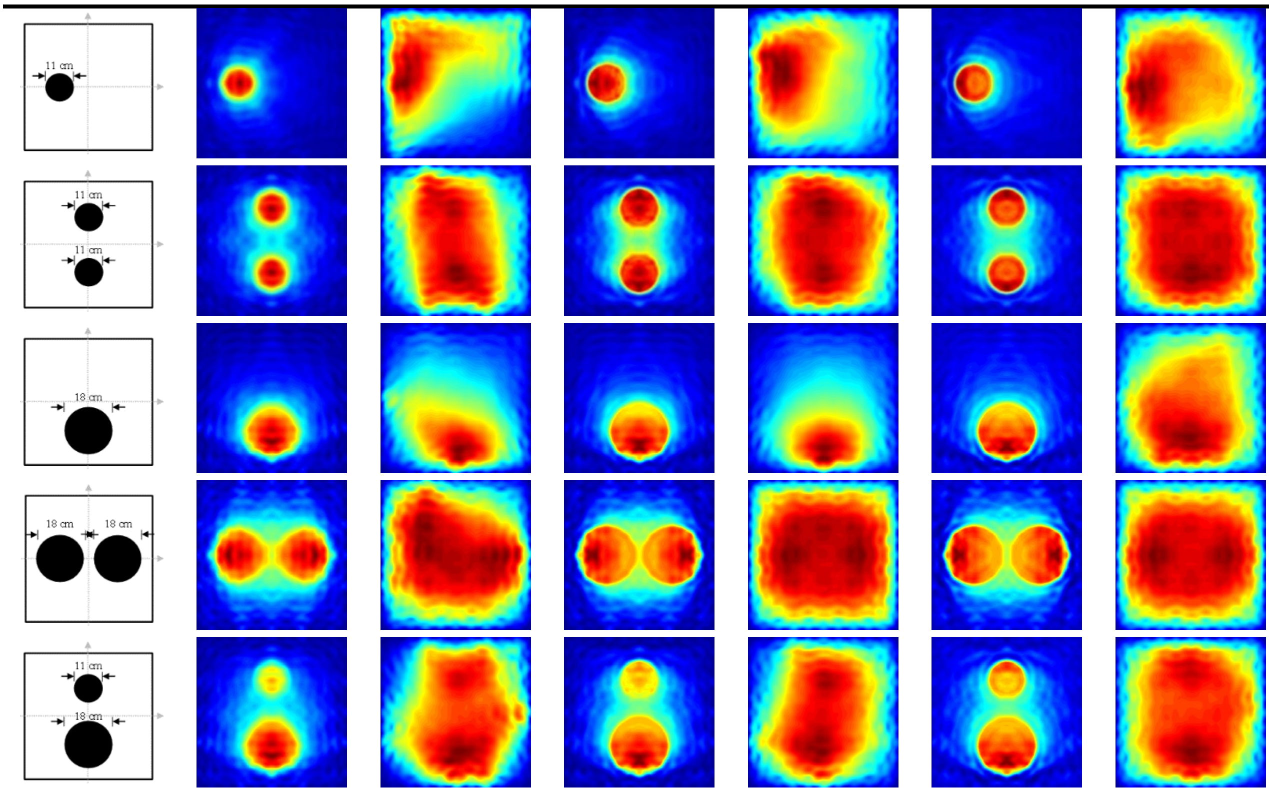

4.1 Image Quality Assessment

Image quality assessment is a tool used to analyse the similarity in terms of visual information of a reconstructed image (tomogram) concerning the reference image (original image). Alternatively, it can be used to determine the suitability of the particular algorithm and the system's efficiency. In this research, the MSSIM index has been employed to quantify the reconstructed images. The MSSIM method compares the structural similarity between two images, producing an output index from 0 to 1. A higher value of the MSSIM index specifies that the reconstructed image is likely identical to the reference image [42, 43]. Tables 6 and 7 show the overall results of the MSSIM index measured on the rice moisture profiles A, B, C, D and E at 15%, 20% and 25% moisture content for both simulation and experimental studies, respectively.

Table 6 *MSSIM indexes measured on the simulation image of rice moisture profiles*

Profile	15% Moisture content				20% Moisture content				25% Moisture content			
	LBP	FBP	NS	TR	LBP	FBP	NS	TR	LBP	FBP	NS	TR
A	0.3523	0.3213	0.4328	0.3928	0.3490	0.3199	0.4331	0.3813	0.3810	0.3419	0.4750	0.4182
B	0.3270	0.3111	0.3800	0.3510	0.3371	0.3201	0.3951	0.3590	0.3599	0.3355	0.4314	0.3883
C	0.3556	0.3361	0.4210	0.3813	0.3678	0.3463	0.4369	0.3948	0.3861	0.3596	0.4601	0.4165
D	0.3912	0.3836	0.4234	0.4049	0.4028	0.3934	0.4407	0.4196	0.4232	0.4077	0.4714	0.4453
E	0.3590	0.3466	0.4069	0.3776	0.3705	0.3559	0.4236	0.3919	0.3927	0.3721	0.4537	0.4188

Int. Journal of Integrated Engineering Vol. 17 No. 2 (2025) p. 222-234

Table 7 *MSSIM indexes measured on the experimental image of rice moisture profiles*

Profile	15% Moisture content				20% Moisture content				25% Moisture content			
	LBP	FBP	NS	TR	LBP	FBP	NS	TR	LBP	FBP	NS	TR
A	0.2895	0.2787	0.3458	0.3004	0.2881	0.2779	0.3115	0.2974	0.2867	0.2776	0.3083	0.2953
B	0.3104	0.2967	0.3330	0.3198	0.3096	0.2994	0.3312	0.3185	0.3080	0.2993	0.3277	0.3160
C	0.3301	0.3136	0.3566	0.3424	0.3267	0.3119	0.3557	0.3405	0.3288	0.3176	0.3496	0.3378
D	0.3918	0.3665	0.4087	0.4002	0.3924	0.3843	0.4067	0.3994	0.3925	0.3843	0.4070	0.3997
E	0.3541	0.3365	0.3773	0.3649	0.3516	0.3318	0.3718	0.3605	0.3506	0.3412	0.3688	0.3589

According to the presented results, the reconstructed images through each image reconstruction algorithm demonstrate decent image quality indexes for all rice moisture levels (15%, 20% and 25%). In the simulation studies, the maximum score of the MSSIM index is 0.4750 at 25% moisture content of Profile A using the NOSER algorithm, whereas the minimum score is 0.3111 at 15% moisture content of Profile B using the FBP algorithm. Based on Table 7, the experimental studies recorded the maximum score of the MSSIM index as 0.4087 at 15% moisture content of Profile D using the NS algorithm, while the minimum score is 0.2776 at 25% moisture content of Profile A using the FBP algorithm.

Regarding the image reconstruction algorithms, the NOSER algorithm constantly recorded the highest MSSIM value among the profile studies, surpassing all the other algorithms throughout the three varying percentages of rice moisture content. In contrast, the lowest MSSIM value is always measured by the FBP algorithm. In this study, the outstanding performance of the NOSER algorithm is potentially due to the iterative step through the measurement from the sensor nodes at the reference distribution model [39]. As reviewed by the previous study, the contradictory imaging results attained by the FBP algorithm are primarily because of the filter matrix that enhances the image noise, which consequently leads to poor image reconstruction accuracy [44].

5. Conclusion

This study successfully designed and developed a novel technique of localization for imaging the rice moisture content distribution in a silo scale based on the tomography method. The development of an RF transceiver sensor array as the tomography sensor for moisture localization and monitoring technique has established a new application of RF tomography sensor, which is independent and adaptable where the RTI system is suitable to be implemented for sizable silo scale measurement. Furthermore, the proposed RTI system has efficiently designed an economical, non-invasive and overall-sensing method for rice moisture distribution without assessing the silo facilities, which eliminates the traditional single-point measurement method. This model has dismissed the complex and destructive procedures.

Acknowledgement

The authors would like to thank Ministry of Higher Education (MOHE) Malaysia for funding this research under the Transdisciplinary Research Grant Scheme (Ref: TRGS/1/2018/UNIMAP/02/4/2). Special acknowledgement goes to Universiti Malaysia Perlis for providing the facilities and technical support.

Conflict of Interest

Authors declare that there is no conflict of interests regarding the publication of the paper.

Author Contribution

The authors confirm contribution to the paper as follows: ***study conception and design:*** *Nurul Amira Mohd Ramli, Mohd Hafiz Fazalul Rahiman, Latifah Munirah Kamarudin, Latifah Mohamed, Ammar Zakaria, Ruzairi Abdul Rahim;* ***data collection:*** *Nurul Amira Mohd Ramli, Mohammed Saeed Moqbel Abdullah;* ***analysis and interpretation of results:*** *Nurul Amira Mohd Ramli, Mohd Hafiz Fazalul Rahiman;* ***draft manuscript preparation:*** *Nurul Amira Mohd Ramli. All authors reviewed the results and approved the final version of the manuscript.*

References

[1] Müller A, Nunes M T, Maldaner V, Coradi P C, Moraes R S de, Martens S, Leal A F, Pereira V F and Marin C K (2022) Rice drying, storage and processing: Effects of post-harvest operations on grain quality Rice Sci. 29 16–30

[2] Postharvest Unit C (2013). Paddy Drying. http://www.knowledgebank.irri.org

[3] Naik D S and Chetti M B (2017) Influence of packaging and storage conditions on the moisture content and its effect on fungal load of paddy Res. J. Agric. Sci. 8 370–374

[4] Alhendi A S, Al-Rawi S H and Jasim A M (2019) Effect of moisture content of two paddy varieties on the physical and cooked properties of produced rice Brazilian J. Food Technol. 22

[5] Firdaus R B R, Tan M L, Rahmat S R and Gunaratne M S 2020 Paddy, rice and food security in Malaysia: A review of climate change impacts Cogent Soc. Sci. 6

[6] You K Y, You L L, Yue C S, Mun K, Yue C S, Mun H K and Lee C Y (2017) Physical and chemical characterization of rice using microwave and laboratory methods Rice - Technology and Production ed Amanullah and S Fahad (InTech) 81–99

[7] Shafiekhani S, Wilson S A and Atungulu G G (2018) Impacts of storage temperature and rice moisture content on color characteristics of rice from fields with different disease management practices J. Stored Prod. Res. 78 89–97

[8] Prakash B, Siebenmorgen T J, Gibson K E and Kumari S (2019) Effect of storage moisture content on miling characteristics of rough rice Trans. ASABE 62 1011–9

[9] Nirmaan A M C, Prasantha B D R, and Peiris B L (2020) Comparison of microwave drying and oven-drying techniques for moisture determination of three paddy (Oryza sativa L.) varieties Chem. Biol. Technol. Agric., 7, 1–7

[10] Vera M, Dutta B, Mercer D G, Maclean H L and Touchie M F (2019) Assessment of moisture content measurement methods of dried food products in small-scale operations in developing countries : A review Trends Food Sci. Technol. 88 484–496

[11] Nath K D and Ramanathan P (2017) Non-destructive methods for the measurement of moisture contents - A review Sens. Rev. 37 71–77

[12] Gilmore C, Asefi M, Paliwal J and LoVetri J (2017) Industrial scale electromagnetic grain bin monitoring Comput. Electron. Agric. 136 210–220

[13] Shukri s and Kamarudin L M (2016) Device free localization technology for human detection and counting with RF sensor networks: A review J. Netw. Comput. Appl. 97 157–174

[14] Wilson J and Patwari N (2010) Radio tomographic imaging with wireless networks IEEE Trans. Mob. Comput. 9 621–632

[15] Mohd Ramli N A, Fazalul Rahiman M H, Kamarudin L M, Mohamed L, Zakaria A, Ahmad A and Rahim R A (2021) A new method of rice moisture content determination using voxel weighting-based from radio tomography images Sensors (Basel). 21

[16] Rahiman M H F (2013) Ultrasonic tomography system for liquid / gas bubble column (Universiti Teknologi Malaysia)

[17] Pawar E 2016 A review article on acrylic PMMA ISOR J. Mech. Civ. Eng. 13 1–4

[18] Obeidat H, Alabdullah A, Elkhazmi E, Suhaib W, OObeidat O, Alkhambashi M, Mosleh M, Ali N, Dama Y, Abidin Z, Abd-Alhameed R and Excell P (2020) Indoor environment propagation review Comput. Sci. Rev 37 100272

[19] Erunkulu O O, Zungeru A M, Lebekwe C K, and Chuma J M (2020) Cellular communications coverage prediction techniques: A survey and comparison IEEE Access 8, 113052–113077

[20] Kiat T T W, Rahiman M H F, Jack S P and Rahim R A (2015) Initial study on microwave technique to find the relationship between attenuation of microwave and thickness of a subject J. Teknologi. 77 99–103

[21] Kiat T T W (2017) Simulation study of tomography for agarwood evaluation (Universiti Malaysia Perlis)

[22] Amineh R K (2020) Applications of electromagnetic waves: Present and future Electron. 9 15–18

[23] Rahiman M H F, Thomas T W K, Soh P J, Rahim R A, Jamaludin J, Ramli M F and Zakaria Z (2019) Microwave tomography sensing for potential agarwood trees imaging Comput. Electron. Agric. 164 104901

[24] Mallach M, Gebhardt P and Musch T (2017) 2D microwave tomography system metal pipes Flow Meas. Instrum. 53 80–88

[25] Wahab Y A, Rahim R A, Leow P L, Rahiman M H F, Ridzuan Aw S, Yunus F R M and Rahim H A (2018) Optimisation of electrode dimensions of ERT for non-invasive measurement applied for static liquid–gas regime identification Sensors Actuators, A Phys. 270 50–64

[26] Kittiamornkul N, Jirasereeamornkul K, Kiattisin S, Chamnongthai K and Higuchi K (2015) The electric field distribution of a hybrid rectangular and circular waveguide resonator for use in granular material dielectric measurements IEEJ Trans. Fundam. Mater. 135 439–49

[27] Hu G (2016) Study on the signal transmission characteristics of 2.4 GHz wireless network in dorms Int. J. Online Eng. 12 58–63

[28] Joo J, Jeong H J and Han D S (2018) Verification of fresnel zone clearance for line-of-sight determination in 5.9 GHz vehicle-to-vehicle communications Wirel. Pers. Commun. 101 239–449

[29] Boukar A J, Daeri A M and Alqusbi E (2016) Effect of antenna height and distance on attenuation for point to point wave propagation 4th International Conference on Control Engineering and Information Technology, CEIT 2016 (IEEE)

[30] Ramli N A M, Rahiman M H F, Malik M F A, Kamarudin L M, Mohamed L, Zakaria A and Abdullah M S M (2020) A design and development of a wireless sensor network for potential monitoring and localization J. Electr. Eng. Technol.

[31] Edwards K, Geddert N, Krakalovich K, Kruk R, Asefi M, Lovetri J, Gilmore C and Jeffrey I (2020) Stored grain inventory management using neural-network-based parametric electromagnetic inversion IEEE Access 8 207182–8207192

[32] Salleh J (2012) Development of monopole sensors for rice quality characterization in Malaysia (Universiti Teknologi Malaysia)

[33] Asefi M, Jeffrey I, LoVetri J, Gilmore C, Card P and Paliwal J (2015) Grain bin monitoring via electromagnetic imaging Comput. Electron. Agric. 119 133–141

[34] Azmi N, Kamarudin L M, Zakaria A, Ndzi D L, Rahiman M H F, Zakaria S M M S and Mohamed L (2021) Rf-based moisture content determination in rice using machine learning techniques Sensors 21 1–20

[35] Almaleeh A A, Zakaria A, Kamarudin L M, Rahiman M H F, Ndzi D L and Ismail I (2022) Inline 3D volumetric measurement of moisture content in rice using regression-based ML of RF tomographic imaging Sensors 22

[36] Dharmadasa M A I M, Gamage C D and Keppitiyagama C I (2019) Radio Tomographic Imaging (RTI) and privacy implications 18th Int. Conf. Adv. ICT Emerg. Reg. ICTer 2018 - Proc. 413–419

[37] Wahab Y A, Rahim R A, Rahiman M H F, Ridzuan Aw S, Yunus F R M, Puspanathan J, Ayob N M N, Leow P L, Rahim H A, Ahmad I L, Jonet A, Chia K S and Tee K S (2017) Inverse problem: Comparison between Linear Back-Projection algorithm and Filtered Back-Projection algorithm in soft-field tomography Int. J. Integr. Eng. 9 32–36

[38] Amirulah R, Muji S Z M, Jabbar M H, Rahim R A, and Rahiman M H F (2017) Digitalization of linear back projection algorithm for FPGA implementation Proc. - 2016 IEEE Conf. Syst. Process Control. ICSPC 2016, December 113–117

[39] Mallach M, Gevers M, Gebhardt P and Musch T (2018) Fast and precise soft-field electromagnetic tomography systems for multiphase flow imaging Energies 2018 11 1–17

[40] Yunos Y M, Rahim R A, Green R G and Rahiman M H F (2007) Image reconstruction using iterative transpose algorithm for optical tomography J. Teknol. 47 91–102

[41] Beck B, Ma X and Baxley R (2016) Ultrawideband tomographic imaging in uncalibrated networks IEEE Trans. Wirel. Commun. 15 6474–6486

[42] Banitalebi-Dehkordi M, Khademi M, Ebrahimi-Moghadam A, and Hadizadeh H (2019) An image quality assessment algorithm based on saliency and sparsity Multimedia Tools and Applications 78 11507–11526

[43] Wang Z, Bovik A C, Sheikh H R and Simoncelli E P (2004) Image quality assessment: From error visibility to structural similarity IEEE Trans. Image Process. 13 600–611

[44] Schofield R, King L, Tayal U, Castellano I, Stirrup J, Pontana F, Earls J and Nicol E (2020) Image reconstruction: Part 1 – understanding filtered back projection, noise and image acquisition J. Cardiovasc. Comput. Tomogr. 14 219–225